Insights Imaging (2010) 1:233–244
DOI 10.1007/s13244-010-0034-7

REVIEW

MR imaging in liver cirrhosis: classical and new approaches

Luis Martí-Bonmatí · Fructuoso Delgado

Received: 16 March 2010 / Revised: 29 June 2010 / Accepted: 12 July 2010 / Published online: 5 August 2010

Abstract
Objective The typical histological features of chronic hepatitis and cirrhosis are variable degrees of hepatocellular necrosis and inflammation (activity or grade of disease), fibrosis (stage of disease), and associated fat and iron deposition. These features influence the liver's appearance and must be assessed separately by imaging biomarkers in order to be clinically useful. Hepatic morphologic alterations and features of portal hypertension identify most cases of established cirrhosis. Nowadays, research is focused on developing ways to improve detection of early and intermediate stages of fibrosis as well as hepatocyte dysfunction. Even more, most imaging-related measurements are subject to complex interactions and are influenced by different pathologic processes, such as fatty infiltration, edema, necrosis and iron accumulation.
Methods and results MR experience throughout the last 15 years at the Dr Peset University Hospital is reviewed.
Conclusion Nowadays, several biomarkers have been developed to grade the liver status in cirrhosis. This review will focus on these topics.

Keywords Liver cirrhosis · Liver, MR imaging

Introduction

Hepatic cirrhosis is a chronic inflammatory liver disorder associated with fibrosis. Although fibrosis is considered the hallmark of cirrhosis, regeneration, necrosis and inflammation are important prognostic factors. Cirrhosis is also frequently associated with steatosis, iron overload and prominent vascular abnormalities.

The most relevant etiologic factors in cirrhosis are alcohol, viruses, nonalcoholic steatohepatitis and hemochromatosis. Initial clinical symptoms are vague, while advanced disease is mainly associated to liver decompensation with ascites, esophageal variceal hemorrhage, jaundice and hepatic encephalopathy. The hepatocellular carcinoma (HCC) development rate is 8% at 5 years and 25% at 10 years.

In most centers, patients with chronic hepatitis and cirrhosis are initially biopsied to establish a definitive diagnosis and stage the liver status. However, a biopsy is not necessary if the clinical, laboratory and radiological data suggest cirrhosis. Furthermore, there is a small but significant risk to liver biopsy, and cirrhosis itself predisposes patients to complications due to liver biopsy.

Magnetic resonance (MR) imaging is mostly used in the diagnosis of tumor development because of its ability to reliably depict HCC. The currently available imaging tests (ultrasound, computed tomography and conventional MR imaging) are neither sensitive nor specific in the detection of early parenchymal changes. Many signs of moderate and advanced cirrhosis can be detected as classical morphological and signal intensity changes. New functional MR imaging sequences can also depict fat and iron deposition, regenerative nodules, necroinflammatory infiltrate, fibrosis, varices, perfusion abnormalities and hepatocyte functionality [1, 2].

The evaluation of chronic hepatitis and cirrhosis with imaging modalities should be performed ideally on early stages of the disease. To be clinically useful, any method used to evaluate chronic hepatitis and cirrhosis must accurately identify regeneration, inflammation, necrosis, fibrosis, fat, iron and also neoplasia. Fibrosis, necroinflammatory activity, fat and iron

L. Martí-Bonmatí (✉) · F. Delgado
Department of Radiology, Dr Peset University Hospital,
Avda Gaspar Aguilar 90. ES 46017 Valencia, Spain
e-mail: Luis.Marti@uv.es

L. Martí-Bonmatí
Department of Radiology, Quirón Hospital,
Avda Blasco Ibáñez 14. ES 46010 Valencia, Spain

deposits are the most important parameters for antiviral treatment indication and follow-up. Report and quantification of these parameters by the radiologist are fundamental in order to entail an impact on patient management.

MR technique

The protocol for MR evaluation of cirrhosis is heavily biased towards HCC depiction. However, the different components of the parenchymal lesions may also need to be studied and quantitated. An all-in-one MR evaluation protocol should include the following sequences.

High-resolution expiratory breath hold dual-echo chemical shift spoiled gradient-echo (GRE) sequencing is used for the acquisition of opposed-phase and in-phase T1-weighted (T1W) images. The dual-echo sequence can evaluate fat, although the use of T2* correction performs better for an accurate quantification [3, 4]. This T2* calculation can be used to measure iron accurately with a multiecho GRE sequence.

Respiratory triggered short T1 inversion recovery turbo spin echo (STIR TSE) images should be optimized so that the signal intensity of the liver is close to that of the subcutaneous fat and paraspinal muscles (TI of 150–160 ms at 1.5-T and 180–190 at 3-T magnets), which serve as an internal tissue of reference for the necro-inflammatory activity.

Three-dimensional spoiled T1W GRE contrast-enhanced dynamic examinations with fat suppression are mainly used to exclude tumor development and grade esophageal varices. Controlling the bolus arrival interval time for the late arterial, portal and equilibrium phases is required. Maximum intensity projection (MIP) vascular map images reconstructed from the arterial and portal phases show the extent of collateral vessels due to portal hypertension, as well as the arteries that perfuse abnormal regions and lesions.

In order to calculate pharmacokinetic model parameters, the acquisition should have enough temporal resolution (less than 5 s for each image set, for at least 5 min) with a dual input double compartment model. A voxelwise statistical analysis is suggested. This dynamic acquisition can be acquired with a low dose of contrast media (a fifth of the regular dose) and also be used to calculate the bolus arrival time to properly initiate the late arterial phase of the high-resolution conventional dynamic sequence.

The 3D high-resolution fat suppression T1W spoiled GRE images obtained 30 to 60 min after the administration of hepatobiliary contrast media (HBCM), although not routinely used in the MR evaluation of cirrhosis and HCC development, may give information on hepatocyte functionality.

The T2* GRE images obtained after superparamagnetic iron oxide particle (SPIO) liver enhancement, with and without concomitant gadolinium-based contrast-enhanced dynamic images, can be used to rule out HCC in difficult cases and depict advanced fibrosis. Specific contrast media with intracellular phases may be used to differentiate perfusion abnormalities from tumor development.

Although large vessels can be observed with most MR images, the use of steady-state fully refocused transverse magnetization GRE images (such as balanced, Fiesta or true-FISP) facilitates the observation of abnormal parenchyma vessels.

Diffusion-weighted (DW) imaging is an MR technique that is based on intravoxel incoherent motion (IVIM) and provides noninvasive quantification of water diffusion and microcapillary-blood perfusion. Information provided with DW reflects tissue cellularity, integrity of cellular membranes and capillarity. In order to standardize DW acquisitions and apparent diffusion coefficient (ADC) calculations, a biexponential signal modeling and respiratory-triggered precontrast acquisitions with at least 5 b-values (0, 50, 200, 400 and 1,000 s/mm2) are suggested [5].

Imaging regeneration

Chronic hepatitis does not modify the macroscopic architecture of the liver. On the other hand, advanced cirrhosis generates typical morphological changes in the liver parenchyma and surface contour because of regenerating nodules, necrosis and fibrous development, which alter the liver architecture.

Liver surface nodularity is usually fine and diffuse, being more prominent on the hypertrophied segments. Although the finding has been claimed as characteristic, minor bulging of the liver surface can be found in normal cases, and also hepatic surface nodularity can be seen in patients with fulminant hepatic failure, usually reflecting a combination of alternating foci of confluent regenerative nodules and necrosis [6].

Regeneration and necrosis lead to liver global or segmental volumetric changes associated with regional variations in the portal venous blood supply [7]. Although any combination can be found, the caudate lobe and lateral segment of the left hepatic lobe usually develop hyperplasia, whereas the left medial segment and right lobe show atrophic changes (Fig. 1a). As a tendency, atrophy is most frequently seen in alcohol-induced cirrhosis.

One of the first imaging biomarkers for diagnosing cirrhosis was the evaluation of caudate lobe hyperplasia with the caudate-right lobe ratio [8]. This index chose the bifurcation of the main portal vein as a reproducible landmark to divide these lobes. A ratio greater than 0.65 is associated with cirrhosis with an overall accuracy of 66%. The modified caudate-right lobe ratio uses the right portal vein bifurcation to set the lateral boundary, with an abnormal index being greater than 0.9. This index is more accurate (74%) for diagnosing cirrhosis and evaluating its clinical severity as significant differences were found

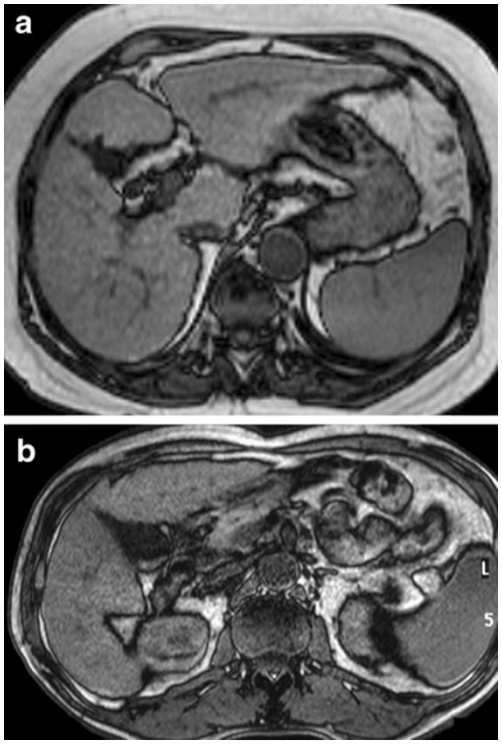

Fig. 1 Morphological changes of the liver. Transverse opposed-phase T1W images show caudate hypertrophy with nodular surface and prominent fat at the hepatic hilum (**a**). The right posterior hepatic notch sign is clearly defined in another patient (**b**)

among the three Child-Pugh classes (Table 1) ($p < 0.01$) [9].

Caudate hypertrophy is also responsible for the right posterior hepatic notch sign, defined as a sharp indentation on the medial posteroinferior liver surface between the caudate and right lobes (Fig. 1b). The deeper the notch, the more advanced the cirrhosis. This finding has a very high positive predictive value [10].

Another associated finding related with segmental parenchyma atrophy is the widening of the porta hepatis demonstrated as a prominent fatty space anterior to the main portal vein at the hepatic hilum. The enlargement of the pericholecystic space (Fig. 2) bounded laterally by the right hepatic lobe and medially by the lateral segment of the left hepatic lobe is

Fig. 2 Morphological changes of the liver. Transverse in-phase T1W image shows an expanded gallbladder fossa sign

known as the expanded gallbladder fossa sign [11]. Again, both signs have a high positive predictive value but much lower sensitivity [12]. The umbilical fissure also widens with the left lobe segmental atrophy. Although all these changes must be considered specific for relatively advanced cirrhosis, the enlargement of the hilar periportal space has been demonstrated in early cirrhosis [11].

Most regenerative nodules are small. Macroregenerative nodules rarely exceed 2 cm in diameter, and therefore larger nodules should be carefully evaluated to exclude dysplasia and carcinogenesis. Slightly hypovascularized large confluent areas of regenerative nodules may be seen mainly close to the interlobar and intersegmental territories.

Regenerative nodules are homogeneous, non-encapsulated, hypointense, rounded foci on T2W images, whereas they are usually isointense on T1W images. They are surrounded by fine reticular septa, slightly hyperintense on fat-suppressed T2W and STIR images (Fig. 3). Markedly hypointense nodules on the in-phase second echo GRE and T2W TSE images are considered siderotic. Some non-dysplastic and non-tumoral nodules may be hyperintense on the T1W GRE images (Fig. 4), but they do not contain fat (do not lose signal intensity on opposed-phase imaging) and are not arterialized (do not significantly enhance during the hepatic arterial dynamic phase). This high signal intensity in T1W images is

Table 1 The Child-Pugh score employs five clinical measures of liver disease. Each measure is scored 1–3, with 3 indicating the most severe derangement. INR = international normalized ratio of prothrombine prolongation

Measure	1 point	2 points	3 points
Total bilirubin (μmol/l and mg/dl in brackets)	<34 (<2)	34–50 (2-3)	>50 (>3)
Serum albumin (g/l)	>35	28–35	<28
INR	<1.7	1.71–2.20	>2.20
Ascites	None	Mild	Severe
Hepatic encephalopathy	None	Grade I–II (or suppressed with medication)	Grade III–IV (or refractory)

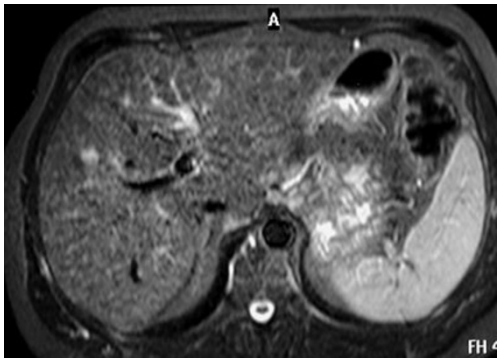

Fig. 3 Fibrosis and regenerative nodules. Transverse STIR image shows a reticular pattern of the fibrotic bands surrounding hypointense regenerative nodules

multifactorial, but mainly related to the intracellular glycogen content [13].

Cirrhosis is not the only disease associated with morphological changes of the liver. Regeneration and atrophy can also be found in disorders such as Budd-Chiari syndrome, postchemotherapy, nodular regenerative hyperplasia and portal cavernomatosis.

Imaging inflammation and necrosis

Standard T1W and T2W images are not sensitive to the inflammatory liver changes. On the contrary, respiratory triggered STIR TSE images depict an increase in liver brightness when there is an increase in the water content due to intracellular edema, inflammation or cell necrosis (Fig. 5). This increased signal can be qualitatively assessed if the inversion time T1 is properly adjusted so that the normal liver signal intensity is quite similar to the signal of the paraspinal muscles. In chronic hepatitis and cirrhosis, this increase in the liver signal intensity can be considered a surrogate marker of portal inflammation and periportal and lobulillar necrosis [14]. The liver signal in STIR images is not influenced by the presence of either fibrosis or steatosis. However, the presence of iron decreases the liver signal intensity and masks the increased signal of the necroinflammatory infiltrates. If iron is present, the necroinflammatory activity cannot be properly estimated with TSE-STIR images.

Reactive lymph nodes at the hepatic hilus and gastrohepatic ligament are also well-known findings. Lymphadenopathy occurred more frequently in autoimmune and virus-induced cirrhosis. Superior diaphragmatic adenopathies are usually hyperplastic, even when an HCC is present (Fig. 6). A prominent cisterna chyli, with a diameter larger than 2 mm, is observed in uncompensated cirrhosis with a high positive predictive value of 96%. This phenomenon is due to the increased lymph production in these patients caused by disturbance in the drainage of vascular flow from the sinusoid

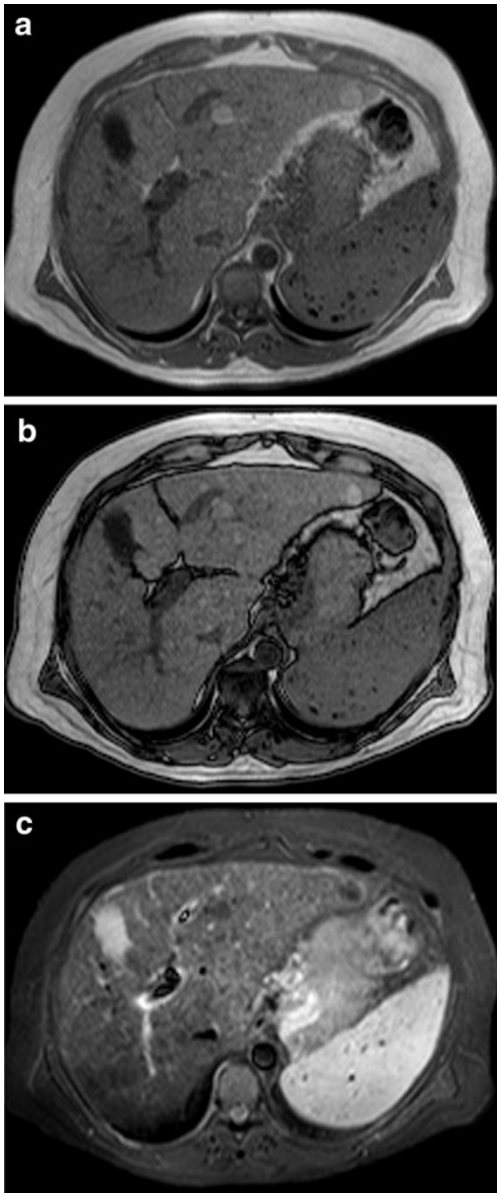

Fig. 4 Non-tumoral nodules. Transverse opposed (**a**) and in-phase (**b**) T1W images show hyperintense nodules without decreased signal intensity on opposed-phase imaging and hypointensity on STIR image (**c**). Note several Gamna-Gandy siderotic splenic bodies due to advanced portal hypertension

to the central or terminal hepatic veins associated with lobular distortion-impaired lymphatic circulation in cirrhosis [15].

Late arterial phase dynamic contrast-enhanced MR images may demonstrate a heterogeneous pattern of patchy parenchymal enhancement with large geographical areas showing a slight hypovascularization [16]. This frequent finding (50%) of perfusion heterogeneity relates to the presence of inflammatory macrophages, variable hepatocyte necrosis and increased steatosis. These areas may progress to areas of focal confluent fibrosis and collapse [17].

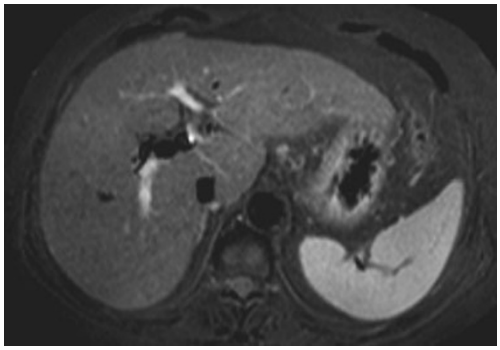

Fig. 5 Inflammation and necrosis. Transverse STIR image shows an increase in liver brightness due to intracellular edema, inflammation and necrosis

In the cellular phase after HBCM, a decreased and heterogeneous enhancement relates to the presence of hepatocyte necrosis intermixed with fibrous bands. Areas of regeneration demonstrate an increased enhancement related to the increase in the number of hepatocytes per voxel together with an impaired bile excretion [18]. In cirrhosis, the severity of the hepatic injury relates to the down-regulation of the HBCM transporter expression, leading to a threshold response appearing in advanced stages (much lower enhancement), but not before (relative maintained enhancement). With this limitation in mind, the Gd-EOB-DTPA hepatic extraction fraction can be used as a direct, noninvasive technique for the quantitative evaluation of liver function. This extraction ratio is calculated from deconvolution analysis of aortic and hepatic parenchymal time-intensity curves obtained by dynamic MRI and could be a promising alternative for the determination of noninvasive hepatic function in patients with liver disease [19].

On the T2*W GRE images acquired with a long TE (≈7 ms), the less hypointense areas are statistically related to reduction in their functional status. Heterogeneous R2* shortening is also a reliable predictor of advanced fibrosis (Fig. 7), with a positive predictive value of 93%. Unfortunately, SPIO measurements are insensitive to early and moderate abnormalities. Iron oxide particles will clearly depict the fibrotic bands surrounding the hypointense negatively enhanced regenerative nodules [20].

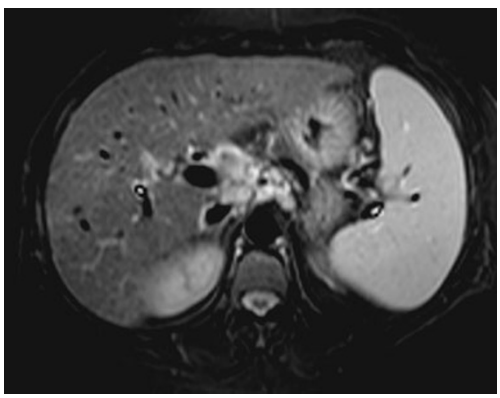

Fig. 6 Reactive lymph node. Transverse STIR image shows lymphadenopathy at the gastroduodenal and retroperitoneal areas. Note the increased signal intensity of the liver due to necroinflammatory activity

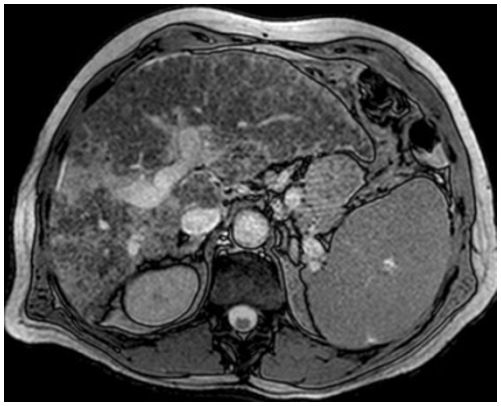

Fig. 7 Fibrosis. Liver heterogeneous decreased enhancement after SPIO is related to the presence of fibrous bands and subcapsular collapse areas

In an early study in patients with liver biopsy, ADC was not correlated with inflammation grades [21]. However, more recent publications [22, 23] have shown a significant relationship between ADC and inflammation scores, with ADC being a predictor of inflammation grade 1 or greater. Unfortunately, ADC values are influenced by the choice of b-value; they are multifactorial (steatosis, fibrosis, perfusion) and vary between different vendors, limiting the role of standard ADC calculations.

Imaging fibrosis

Routine MR imaging cannot observe early fibrosis, but these images are sensitive for detecting moderate and advance fibrosis by demonstrating the reticular pattern of the fibrotic bands surrounding regenerative nodules. This fine reticulation is hyperintense on T2W fat-suppressed images and on the equilibrium and delayed images after contrast administration (Fig. 8). This appearance is due to the coexistence of inflammation in these fibrotic areas. The fine sieve appearance, occasionally associated with poorly defined subcapsular retractile stellate areas, are clear indicators of the presence of advanced fibrosis. Confluent mass-like lesions may also be depicted. The observation of this pattern is facilitated by decreasing the signal intensity of the nodules after SPIO administration while increasing the signal from the septa after gadolinium enhancement [2]. This double contrast technique has been shown to be accurate for advanced fibrosis [24]. Although this method separates advanced fibrosis or cirrhosis (F3–F4) from intermediate, early or no fibrosis (F2-F0), it

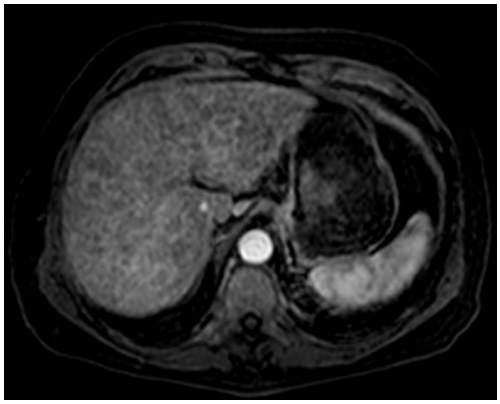

Fig. 8 Fibrosis. Transverse fat suppression T1W spoiled GRE image after administration of contrast media shows reticular pattern of the fibrotic bands surrounding regenerative nodules

does not allow to differentiate no fibrosis (stage F0) from minimal (stage F1) and intermediate (stage F2) fibrosis.

Areas of focal confluent fibrosis are usually found in long-standing cirrhosis, especially associated with alcohol abuse. They are frequently multiple, with the most classical locations being the interlobar and intersegmental fissures, as these areas have terminal territory perfusion. The collapsed area has a geometrical (often triangular or quadrilateral) capsular-based wedge shape pointing to the hepatic hilum, associating volume loss and capsular retraction with focal flattening or even concavity of the adjacent liver surface. The abnormality is moderately hyperintense in T2W images, isointense or slightly hypointense in T1W, with a progressive and delayed enhancement after contrast media administration (Fig. 9). Trapped vessels and dilated biliary ducts can be seen within the abnormality. On the cellular phase images after HBCM and SPIO administration, the enhancement is usually decreased due to cell necrosis. Internal focal areas of contrast pooling correspond to residual functioning liver parenchyma.

Microscopic water diffusion is decreased in cirrhosis [2]. The reduced liver diffusion can be qualitatively observed on the DW images (Fig. 10). Some studies have analyzed the role of DW imaging, mainly throughout mean ADC comparisons, in the evaluation of chronic diffuse liver diseases. Although ADC measurements vary in b-values and motion correction techniques, the ADC values of cirrhotic livers are significantly lower. The shortest ADC values in cirrhosis are mainly related to a decrease in the capillarity perfusion component and not to a true microscopic diffusion restriction associated with fibrosis and inflammation [25].

Taouli et al. evaluated DW technique as a predictor of the presence of moderate and advanced liver fibrosis [26]. The liver ADC value (breath hold, six b-values of 0, 50, 300, 500, 700 and 1,000 s/mm^2) in patients with chronic hepatitis versus healthy volunteers was a significant predictor of fibrosis stage F2 or greater and also stage F3 or greater. Similar results were

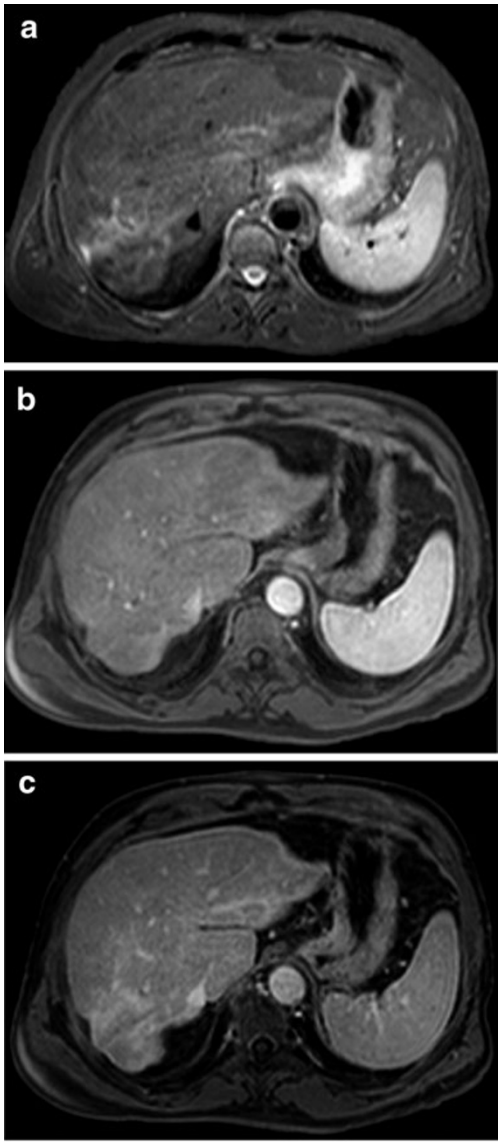

Fig. 9 Focal confluent fibrosis. STIR image shows a collapsed area with capsular-based wedge shape. The abnormality is moderately hyperintense in STIR (**a**) and shows progressive and delayed enhancement after contrast media administration (**b**, arterial; **c**, delayed phases)

obtained by Lewin et al., where DW (navigator-triggered, four b-values: 0, 200, 400, and 800 s/mm^2) was compared to other non-invasive methods to conclude that patients with moderate-to-severe fibrosis (F2-F3-F4) had hepatic ADC values lower than those without or with mild fibrosis (F0-F1) and healthy volunteers [22]. In discriminating patients staged F3-F4, the sensitivity, specificity, positive predictive value and negative predictive value were 87%, 87%, 72% and 94%, respectively, with an ADC cutoff level of 1.21×10-3 mm^2/s.

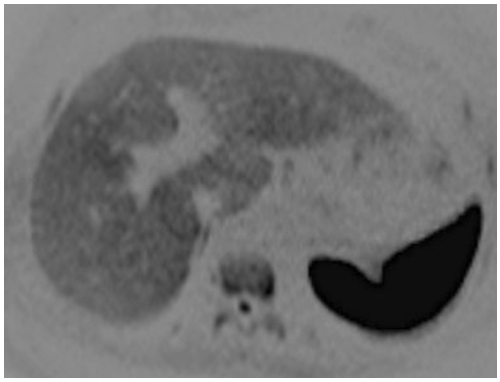

Fig. 10 Fibrosis. Transverse signal video inversion of the diffusion-weighted image shows decreased water diffusion in a patient with liver cirrhosis

Luciani et al. analyzed the influence of fibrosis in liver diffusion properties by IVIM technique (respiratory triggered, ten b-values: 0, 10, 20, 30, 50, 80, 100, 200, 400, 800 s/mm^2). They observed a restricted diffusion in patients with cirrhosis mainly related to variations in the perfusion component, reflecting decreased perfusion, as well as alterations in pure molecular water diffusion in cirrhotic livers [27]. Confirming this observation, Girometti et al. (breath hold acquisition; six b-values: 0, 150, 250, 400, 600, 800 s/mm^2) also concluded that the perfusion component presents a higher accuracy at lower b-values for the assessment of liver fibrosis [28]. The studies in rats with hepatic fibrosis, both in-vivo and immediately after death, also pointed in this direction [25].

Although IVIM seems to be a promising technique in the diagnosis and staging of fibrosis, some bias must be clearly controlled to standardize this biomarker (Fig. 11). The concomitant effect of MR machines, MR sequence parameters, fat, iron, inflammation and necrosis on the ADC values should be evaluated.

Cirrhotic liver vascular perfusion changes are related to the disease activity and staging [2]. Although the arterial blood supply is increased due to the decreased portal flow, the buffer is not sufficient to maintain adequate liver perfusion because of the high level of extrahepatic portosystemic shunting. The overall reduction of the total liver perfusion can be quantified as a prolongation of the mean transit time and a decrease in mean peak liver enhancement.

Another phenomenon is observed as fibrosis development leads to progressive arterializations of the hepatic sinusoidal bed, with shunting and hyperdynamic circulation, and augmentation of the extracellular interstitial space with collagen deposition. These changes produce an overall increase of the liver enhancement during the equilibrium phase images of the dynamic series. Some parametric pixel-by-pixel mapping, such as the mean and maximum enhancement ratios, show significantly higher values in cirrhosis than in normal livers [16]. An increase in the liver enhancement can also be also quantified with the area under the curve and is statistically related to the degree of chronic hepatic insufficiency. A dual-input single compartment model demonstrates an increased distribution volume (related to the increased interstitial volume) and mean transit time (related to the collagen deposition in the extracellular spaces of Disse) [29].

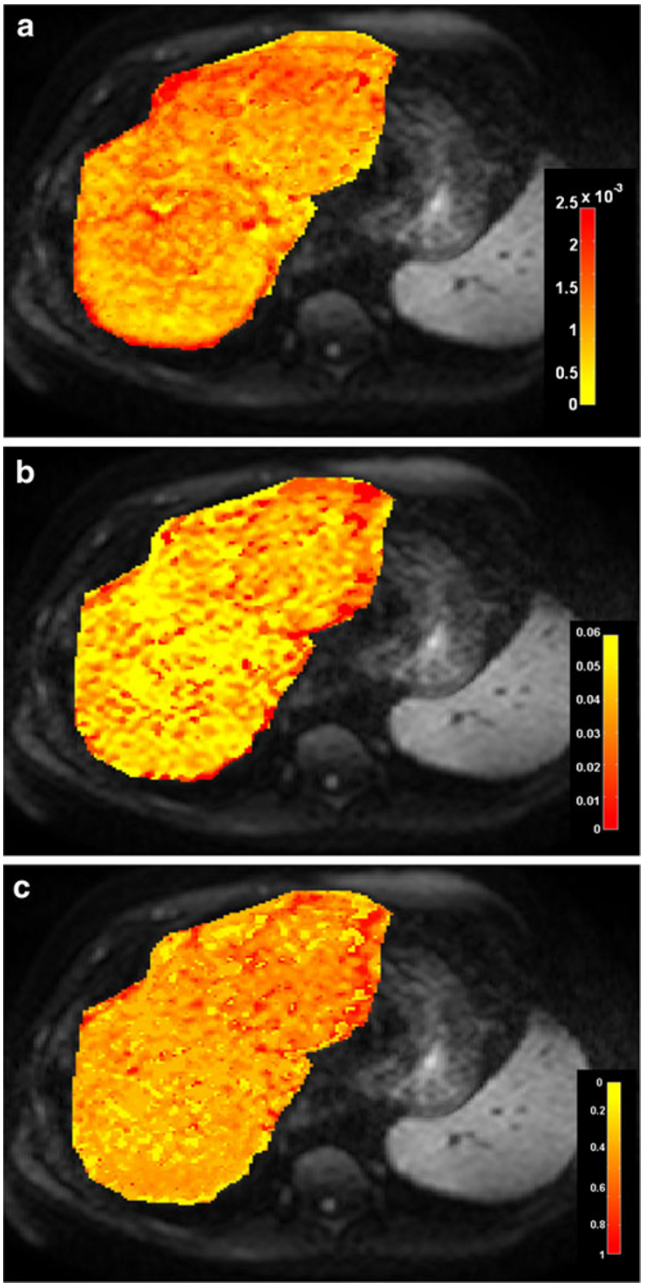

Fig. 11 Fibrosis. IVIM parametric maps of pure diffusion (**a**, **d**), perfusion (**b**, **d***) and vascular components (**c**, **f**) of the diffusion-related signal attenuation

These perfusion modifications can be separated and objectively evaluated through the pharmacokinetic compartment model analyses. Although the experience is limited, cirrhotic livers have an increased vascular permeability (K^{trans}) and extracellular space (υ_e) with a heterogeneous distribution. These parameters correlate with the degree of liver fibrosis and may be used as a hemodynamic biomarker in injured fibrotic livers.

MR elastography uses a sound wave generator applied to the patient [30]. The shear mechanical compressional waves are transmitted through the liver, detected with phase-contrast type sequences, and analyzed as wave propagation and tissue deformation. The calculated elasticity maps show the shear elasticity modulus (kPa) at each point. Quantitative stiffness parametric maps, also known as elastograms, become more heterogeneous with increasing fibrosis. Liver stiffness increases as the stage of fibrosis advances. While differences in stiffness between patients with early stages of fibrosis (F0 vs. F1 vs. F2) are small, with overlap between groups, the differences between higher stages (F2 vs. F3 vs. F4) are larger with less overlap [31].

MR spectroscopy enables the in vivo noninvasive quantization of some biochemical compounds. Single voxel proton hepatic MR spectroscopy can be obtained with sufficient quality. Glutamine and glutamate complex (Glx), phosphomonoesters (PME), glycogen and glucose complex (Glyu), and lipids are clearly observed. Chronic hepatitis and cirrhosis showed an increase in Glx, PME and Glyu levels relative to the lipid content. This increase is related to the severity of fibrosis, although data overlap is present between groups [32].

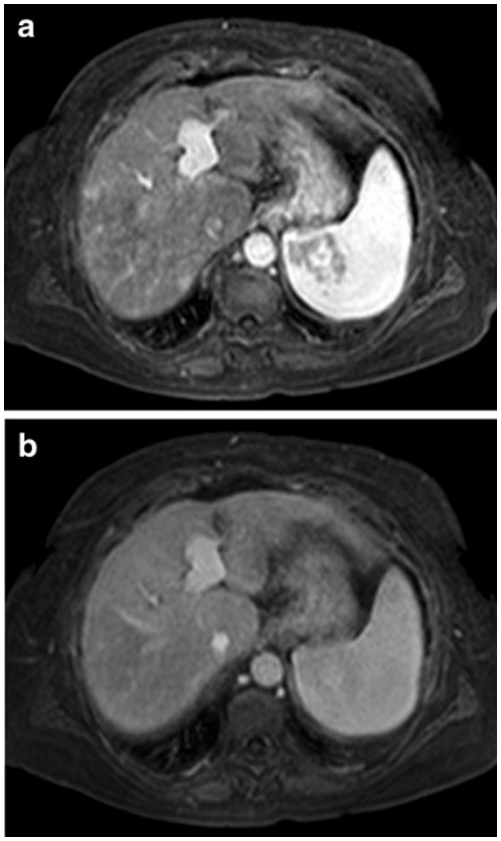

Fig. 12 Vascular changes: arterioportal shunts. Transverse fat suppression T1W spoiled GRE image after administration of contrast media shows small and non-encapsulated areas with enhancement in the arterial phase (**a**), but without wash-out on the portal phase image (**b**)

Imaging vascular changes

Early fibrosis associates deposition of collagen in the Disse space with alteration of the sinusoidal architecture, resulting in a decreased portal venous flow, which is counteracted by an increase in hepatic arterial flow (buffer response). When the venous inflow blockade occurs and vascular resistance increases, the portal flow may be adequate for centrally located parenchyma areas, but not for the subcapsular regions. The arterial response may generate enhancement of these peripheral zones with relative hypointensity in the central perihilar areas.

On the contrary, as previously mentioned, there may also be a heterogeneous pattern of slightly hypervascular behavior within geographical areas due to the presence of necroinflammatory infiltrates and steatosis [33]. Other common causes of perfusion abnormalities to be taken into consideration in cirrhotic livers are related to spontaneous arterioportal shunts (Fig. 12), shunts associated with vascular compression (HCC, inflammatory changes, biliary tree dilatation) and portal occlusion [34].

Portal hypertension frequently complicates liver cirrhosis. Dilatation of the portal vein and its tributaries, and extrahepatic collateral circulation, splenomegaly and ascites are well-known findings. Esophageal and gastric varices, paraumbilical, spleno-renal, retroperitoneal and puborectal shunts are well visualized with contrast-enhanced MR images and MIP projections (Fig. 13). MR images after Gd administration depict esophageal varices in most (81%) cases with a statistically significant relationship with the endoscopic grading of the severity [35]. Vascular engorgement of the mesenteric vessels may produce a pseudoomental cake appearance. Gallbladder wall thickening is associated with venous and lymphatic congestion in the presence of portal hypertension and drainage difficulty [36].

A relatively small main portal vein in patients with cirrhosis may indicate hepatofugal flow. Early arterial phase enhancement of the portal vein has been also reported as a sign of hepatofugal flow [37], although this finding is misleading as the late arterial phase mixes with the early portal phase.

In most cases, perfusion abnormalities are easy to interpret on the non-specific contrast media enhanced images as they

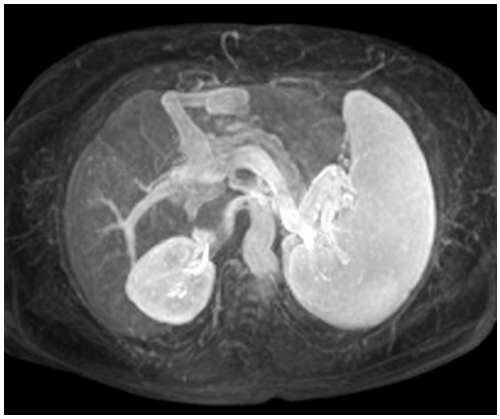

Fig. 13 Portal hypertension. MIP vascular image reconstructed from the portal phase shows collaterals vessels and splenomegaly

have clearly defined and straight-line margins, corresponding to a vascular territory, and normal vessels coursing through the abnormality. When the portal flow is decreased or absent and the arterial flow volume is increased, they are often seen as hyperarterialization with fading or disappearance in the portal and equilibrium phases [38].

Imaging biliary changes

Liver cirrhosis may result in peribiliary cysts. Cyst abnormalities occur in the peribiliary tissue adjacent to the large intrahepatic and extrahepatic ducts in association with severe liver disease, and are usually asymptomatic [39]. These cysts have variable size and morphology and represent cystic dilatation of the extramural glands in the periductal connective tissue. Peribiliary cysts show imaging findings of simple cysts, with low signal intensity on T1W and high signal on heavily T2W MR images (Fig. 14).

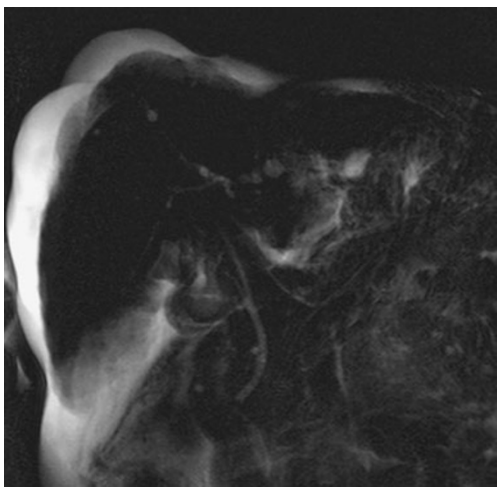

Fig. 14 Liver peribiliary cysts. MRCP image shows peribiliary cysts with variable size and morphology

Primary sclerosing cholangitis (PSC) shows irregular intra- and/or extrahepatic bile duct dilatation and stenosis along with periportal T2W hyperintensity in the major portal tracts. Cirrhosis from advanced PSC develops marked atrophy of the posterior aspect of the right lobe and the lateral segment of the left lobe with hypertrophy of the caudate lobe.

In primary biliary cirrhosis, intrahepatic bile ducts are progressively destroyed because of chronic non-suppurative cholangitis. On T2W images, a periportal hyperintensity, especially at earlier stages of disease, may be seen [40].

Imaging fat

Cirrhotic livers may have an increase in fat content. Also, steatosis and nonalcoholic steatohepatitis (NASH) lead to fibrosis and cirrhosis [41]. Early detection and follow-up of steatosis would facilitate a better diagnosis and intervention before liver damage is irreversible [2]. A large number of patients with NASH and chronic hepatitis may also present increased iron content in the liver with all these factors affecting the imaging signal characteristics.

Chemical shift T1W dual echo GRE images (Fig. 15) allow the qualitative diagnosis of steatosis [42]. For the quantitative

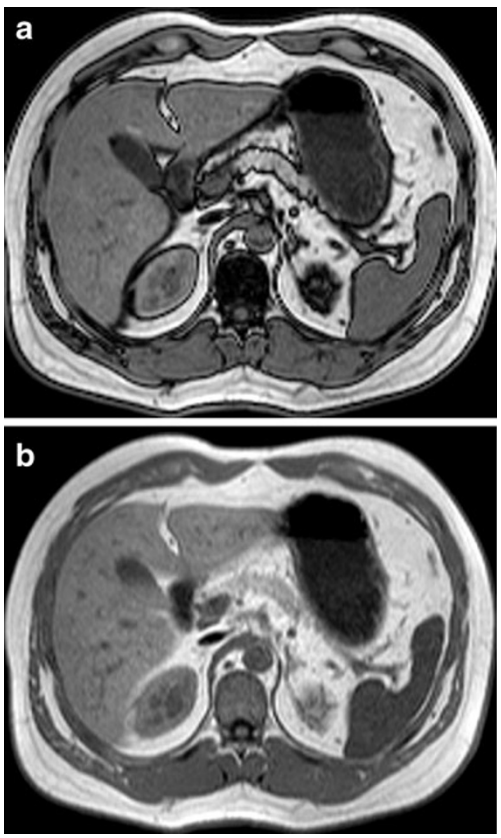

Fig. 15 Liver steatosis. Transverse opposed-phase T1W image (**a**) shows decreased signal intensity of liver, while in the axial in-phase T1W image (**b**) the liver shows increased signal intensity

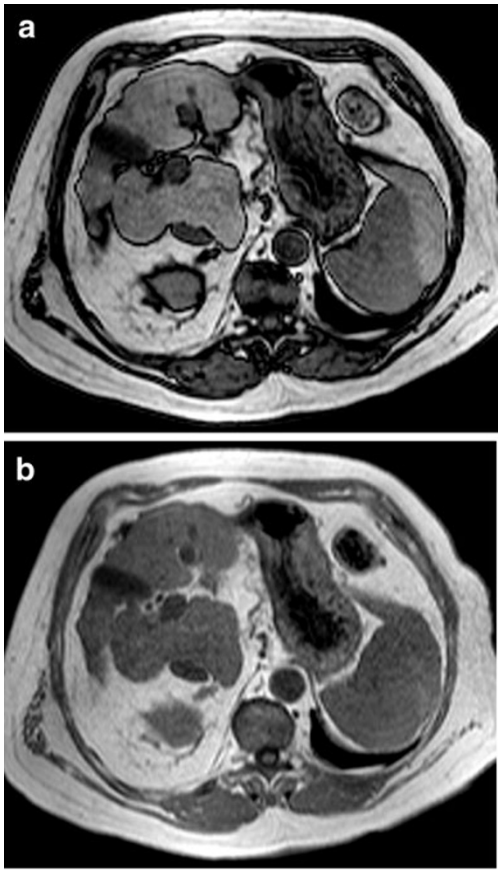

Fig. 16 Liver iron overload. Transverse opposed-phase (**a**) and in-phase (**b**) T1W images show a decrease in the signal intensity of the liver in the in-phase image because of increased deposition of iron

evaluation, the fat content computed from in-phase and opposed-phase images may be erroneous unless a correction is made for the influence of T2* decay [43]. The T2W TSE with and without fat suppression method is easier and accurate enough in a clinical setting [44]. However, single voxel proton MR spectroscopy, although limited by the volume sampling, will be needed in clinical trials and longitudinal studies to further increase accuracy.

Imaging iron

Cirrhosis is frequently associated with an increased deposition of iron, mainly in alcoholic cirrhosis. Also, primary iron overload may lead to cirrhosis. Conventional chemical shift dual echo GRE T1W and TSE-STIR images will demonstrate the liver signal intensity drop, allowing the qualitative diagnosis of significant iron deposits (Fig. 16). When iron has been demonstrated, a quantitative measurement should be obtained.

Both the liver-to-muscle signal ratio and the liver R2* relaxation rate significantly correlate with the amount of

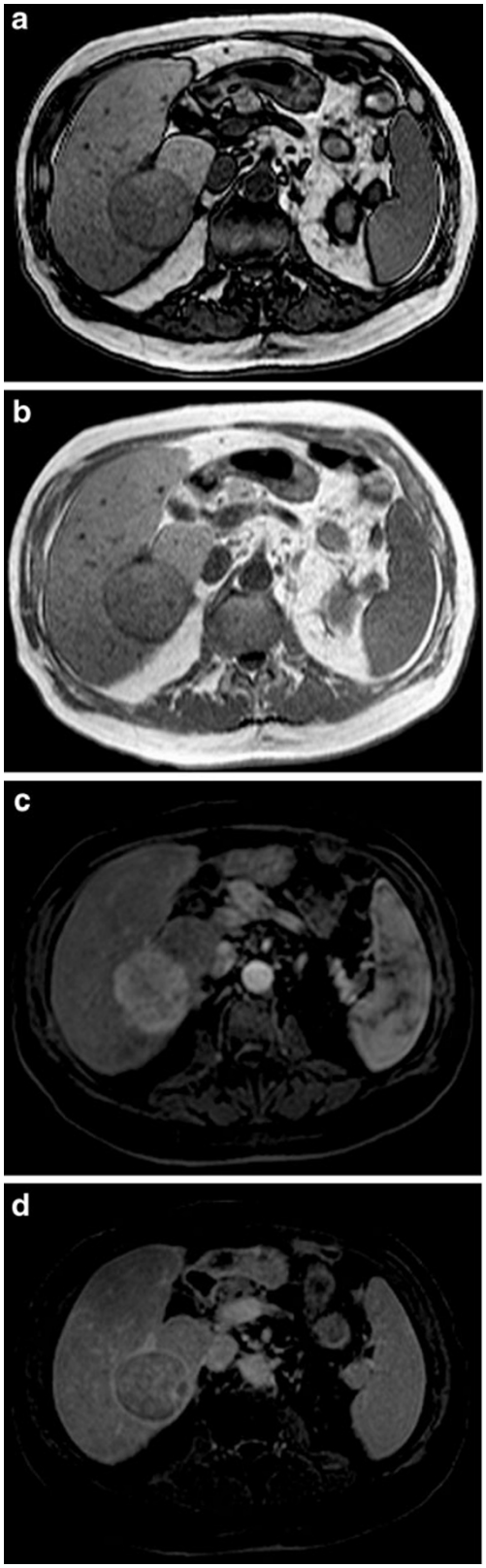

Fig. 17 Hepatocellular carcinoma. Transverse T1W images (**a**, opposed phase; **b**, in-phase) show a slightly hypointense encapsulated lesion located in the right posteroinferior segment. The lesion is hypervascular (**c**) with washout (**d**) with a delayed enhancing outer rim capsule

iron content [3, 4]. Although sequences and postprocessing of images for T2 and T2* relaxation rate calculations are more difficult to implement in a clinical environment, this approach must be preferred to the simple signal-to-ratio determination in clinical trials. The calibration between R2* and iron concentration is dependent on field strength, being different for 1.5- and 3-T magnets [45].

The coupling of multiecho GRE techniques with chemical shift imaging may simultaneously evaluate both iron and fat liver content [46]. This is relevant as both entities may coexist in a significant number of cases with chronic liver disease.

Imaging neoplasia

Liver imaging evaluation in cirrhotic patients should also search for tumor development [47]. Overt HCC is characterized by a mass lesion showing hyperarterialization with washout, becoming hypointense to the liver on the delayed phases after contrast administration (Fig. 17). The presence of a capsule and internal mosaic appearance are secondary criteria. Dysplasia, atypia and early neoplasic degeneration are much more difficult to demonstrate. In this setting, any hyperintensity within a nodule in the T2W images and hyperintense nodules in the T1W images may be considered suspicious, and their perfusion characteristics should be carefully evaluated. DW images may help in depicting a malignant transformation if clear diffusion restriction is observed.

Some special situations in cirrhotic livers need further comment. Nodular appearance of arterio-portal shunts is typically seen in cirrhosis as a small and non-encapsulated area with ill-defined margins. They are not seen on the plain non-contrast-enhanced images, delayed equilibrium and cellular phases after HBCM and reticuloendothelial system contrast media (RECM), allowing the differentiation with small HCC.

To differentiate a nodular arterio-portal shunt from a small HCC without washout on the equilibrium phase images, specific contrast media (either HBCM or SPIO) can be useful if no significantly different uptake is seen, a finding typical of arterio-portal shunt. A transient hepatic arterialization may highlight a small HCC determining portal compression. This is also the situation with peribiliary transient hepatic arterialization caused by long-standing biliary obstruction.

Conclusion

The typical histological features of chronic hepatitis and cirrhosis influence the liver's appearance and must be assessed separately by imaging biomarkers in order to be useful clinically. With advancements in MR technological quantification, several biomarkers have been developed to grade the liver status in cirrhosis. Nowadays, research is focused on developing ways to improve detection of early and intermediate stages of fibrosis as well as hepatocyte dysfunction. The implementation of these biomarkers in a clinical environment is still waiting on an appropriate evaluation of their diagnostic accuracy.

References

1. Talwalkar JA, Yin M, Fidler JL, Sanderson SO, Kamath PS, Ehman RL (2008) Magnetic resonance imaging of hepatic fibrosis: emerging clinical applications. Hepatology 47:332–342
2. Taouli B, Ehman RL, Reeder SB (2009) Advanced MRI methods for assessment of chronic liver disease. Am J Roentgenol 193:14–27
3. Gandon Y, Olivié D, Guyader D, Aubé C, Oberti F, Sebille V, Deugnier Y (2004) Non-invasive assessment of hepatic iron stores by MRI. Lancet 363:357–362
4. Alustiza JM et al (2004) MR quantification of hepatic iron concentration. Radiology 230:479–484
5. Martí-Bonmatí L, Alberich-Bayarri A, Sanz-Requena R, Sánchez-González J. State of the art in liver imaging—MR diffusion/perfusion. Controversies and consensus in imaging and intervention, 2009. http://www.c2i2.org/web09-05/state_of_the_art_in_liver_imaging.asp
6. Poff JA, Coakley FV, Qayyum A, Yeh BM, Browne LW, Merriman RB, Ferrell LD, Feldstein VA (2008) Frequency and histopathologic basis of hepatic surface nodularity in patients with fulminant hepatic failure. Radiology 249:518–523
7. Brancatelli G, Federle MP, Ambrosini R et al (2007) Cirrhosis: CT and MR imaging evaluation. Eur J Radiol 61:57–69
8. Harbin WP, Robert NJ, Ferrucci JJ et al (1980) Diagnosis of cirrhosis based on regional changes in hepatic morphology: a radiological and pathological analysis. Radiology 135:273–283
9. Awaya H, Mitchell DG, Kamishima T, Holland G, Ito K, Matsumoto T (2002) Cirrhosis: modified caudate-right lobe ratio. Radiology 224:769–774
10. Ito K, Mitchell D (2003) Right posterior hepatic notch sign: a simple diagnostic MR finding of cirrhosis. J Magn Reson Imaging 18:561–566
11. Ito K, Mitchell DG, Gabata T, Hussain SM (1999) Expanded gallbladder fossa: simple MR imaging sign of cirrhosis. Radiology 211:723–726
12. Ito K, Mitchell DG (2000) Hepatic morphologic changes in cirrhosis: MR imaging findings. Abdom Imaging 25:456–461
13. Willatt JM, Hussain HK, Adusumilli S, Marrero JA (2008) MR Imaging of hepatocellular carcinoma in the cirrhotic liver: challenges and controversies. Radiology 247:311–330
14. Martí-Bonmatí L, Talens A, del Olmo J, de Val A, Serra MA, Rodrigo JM, Ferrández A, Torres V, Rayón M, Vilar JS (1993) Chronic hepatitis and cirrhosis: evaluation by means of MR imaging with histologic correlation. Radiology 188:37–43
15. Verma SK, Mitchell DG, Bergin D, Lakhman Y, Austin A, Verma M, Assis D, Herrine SK, Parker L (2009) Dilated cisternae chyli: a sign of uncompensated cirrhosis at MR imaging. Abdom Imaging 34:211–216
16. Martí-Bonmatí L. MR contrast agents in hepatic cirrhosis and chronic hepatitis Seminars in Ultrasound, CT, and MRI, 2002; 23:101-113.

17. Brancatelli G, Baron RL, Federle MP, Sparacia G, Pealer K (2009) Focal confluent fibrosis in cirrhotic liver: natural history studied with serial CT. AJR 192:1341–1347
18. Martí-Bonmatí L, Lonjedo E, Poyatos C, Casillas C (1998) MnDPDP enhancement characteristics and differentiation between cirrhotic and noncirrhotic livers. Invest Radiol 33:717–722
19. Ryeom HK, Kim SH, Kim JY, Kim HJ, Lee JM, Chang YM, Kim YS, Kang DS (2004) Quantitative evaluation of liver function with MRI using Gd-EOB-DTPA. Korean J Radiol 5:231–239
20. Tomita K et al (2008) Evaluating the severity of nonalcoholic steatohepatitis with superparamagnetic iron oxide-enhanced magnetic resonance Imaging. J Magn Reson Imaging 28:1444–1450
21. Koinuma M, Ohashi I, Hanafusa K, Shibuya H (2005) Apparent diffusion coefficient measurements with diffusion-weighted magnetic resonance imaging for evaluation of hepatic fibrosis. J Magn Reson Imaging 22:80–85
22. Lewin M, Poujol-Robert A, Boëlle PY, Wendum D, Lasnier E, Viallon M, Guéchot J, Hoeffel C, Arrivé L, Tubiana JM, Poupon R (2007) Diffusion-weighted magnetic resonance imaging for the assessment of fibrosis in chronic hepatitis C. Hepatology 46:658–665
23. Taouli B, Chouli M, Martin AJ, Qayyum A, Coakley FV, Vilgrain V (2008) Chronic hepatitis: role of diffusion-weighted imaging and diffusion tensor imaging for the diagnosis of liver fibrosis and inflammation. J Magn Reson Imaging 28:89–95
24. Aguirre DA, Behling CA, Alpert E, Hassanein TI, Sirlin CB (2006) Liver fibrosis: noninvasive diagnosis with double contrast material-enhanced MR imaging. Radiology 239:425–437
25. Annet L, Peeters F, Abarca-Quinones J, Leclercq I, Moulin P, Van Beers BE (2007) Assessment of diffusion-weighted MR imaging in liver fibrosis. J Magn Reson Imaging 25:122–128
26. Taouli B, Tolia AJ, Losada M et al (2007) Diffusion-weighted MRI for quantification of liver fibrosis: preliminary experience. AJR Am J Roentgenol 189:799–806
27. Luciani A, Vignaud A, Cavet M, Nhieu JT, Mallat A, Ruel L, Laurent A, Deux JF, Brugieres P, Rahmouni A (2008) Liver cirrhosis: intravoxel incoherent motion MR imaging–pilot study. Radiology 249:891–899
28. Girometti R, Furlan A, Esposito G, Bazzocchi M, Como G, Soldano F, Isola M, Toniutto P, Zuiani C (2008) Relevance of b-values in evaluating liver fibrosis: a study in healthy and cirrhotic subjects using two single-shot spin-echo echo-planar diffusion-weighted sequences. J Magn Reson Imaging 28:411–419
29. Hagiwara M, Rusinek H, Lee VS, Losada M, Bannan MA, Krinsky GA, Taouli B (2008) Advanced liver fibrosis: diagnosis with 3D whole-liver perfusion MR imaging—initial experience. Radiology 246:926–934
30. Rouviere O, Yin M, Dresner MA et al (2006) MR Elastography of the liver: preliminary results. Radiology 240:440–448
31. Faria SC, Ganesan K, Mwangi I, Shiehmorteza M, Viamonte B, Mazhar S, Peterson M, Kono Y, Santillan C, Casola G, Sirlin CB (2009) MR imaging of liver fibrosis: current state of the art. Radiographics 29:1615–1635
32. Qayyum A (2009) MR spectroscopy of the liver: principles and clinical applications. Radiographics 29:1653–1664
33. Semelka RC, Chung JJ, Hussain SM, Marcos HB, Woosley JT (2001) Chronic hepatitis: correlation of early patchy and late linear enhancement patterns on gadolinium-enhanced MR images with histopathology initial experience. J Magn Reson Imaging 13:385–391
34. Torabi M, Hosseinzadeh K, Federle MP (2008) CT of nonneoplastic hepatic vascular and perfusion disorders. Radiographics 28:1967–1982
35. Matsuo M, Kanematsu M, Kim T, Hori M, Takamura M, Murakami T, Kondo H, Moriyama N, Nakamura H, Hoshi H (2003) Esophageal varices: diagnosis with gadolinium-enhanced MR imaging of the liver for patients with chronic liver damage. AJR Am J Roentgenol 180:461–466
36. Marti-Bonmati L, Andres JC, Aguado C (1989) Sonographic relationship between gallbladder wall thickness and the etiology of ascites. J Clin Ultrasound 17:497–501
37. Bryce TJ, Yeh BM, Qayyum A, Pacharn BNM, Lu Y, Coakley FV (2003) CT signs of hepatofugal portal venous flow in patients with cirrhosis. AJR 181:1629–1633
38. Colagrande S, Centi N, Galdiero R, Ragozzino A (2007) Transient hepatic intensity differences: part 2, those not associated with focal lesions. AJR 188:160–166
39. Baron RL, Campbell WL, Dodd GD III (1994) Peribiliary cysts associated with severe liver disease: imaging-pathologic correlation. AJR 162:631–636
40. Kobayashi S, Matsui O, Gabata T (2005) MRI findings of primary biliary cirrhosis: correlation with Scheuer histologic staging. Abdom Imaging 30:71–76
41. Lall CG, Aisen AM, Bansal N, Sandrasegaran K (2008) Nonalcoholic fatty liver disease. AJR 190:993–1002
42. Borra RJ et al (2009) Nonalcoholic fatty liver disease: rapid evaluation of liver fat content with in-phase and out-of-phase MR imaging. Radiology 250:130–136
43. Westphalen AC, Qayyum A, Yeh BM et al (2007) Liver fat: effect of hepatic iron deposition on evaluation with opposed-phase MR imaging. Radiology 242:450–455
44. Qayyum A, Goh JS, Kakar S, Yeh BM, Merriman RB, Coakley FV (2005) Accuracy of liver fat quantification at MR imaging: comparison of out-of-phase gradient-echo and fat-saturated fast spin-echo techniques—initial experience. Radiology 237:507–511
45. Fenzi A, Bortolazzi M, Marzola P et al (2003) Comparison between signal-to-noise ratio, liver-to-muscle ratio, and 1/T2 for the noninvasive assessment of liver iron content by MRI. J Magn Reson Imaging 17:589–592
46. Yu H et al (2007) Multiecho reconstruction for simultaneous water-fat decomposition and T2* estimation. J Magn Reson Imaging 26:1153–1161
47. Forner A, Ayuso C, Isabel Real M, Sastre J, Robles R, Sangro B, Varela M, de la Mata M, Buti M, Martí-Bonmatí L, Bru C, Tabernero J, Llovet JM, Bruix J (2009) Diagnosis and treatment of hepatocellular carcinoma. Med Clin (Barc) 132:272–287